

Pressure-driven membrane inflation through nanopores on the cell wall

Qi Zhong(钟祺), Chen-Xu Wu(吴晨旭), and Rui Ma(马锐)

Citation: Chin. Phys. B, 2023, 32 (**8**): 088704. DOI: 10.1088/1674-1056/acd7cc
Journal homepage: http://cpb.iphy.ac.cn; http://iopscience.iop.org/cpb

What follows is a list of articles you may be interested in

Regulation of the intermittent release of giant unilamellar vesicles under osmotic pressure

Qi Zhou(周琪), Ping Wang(王平), Bei-Bei Ma(马贝贝), Zhong-Ying Jiang(蒋中英), and Tao Zhu(朱涛)
Chin. Phys. B, 2022, 31 (**9**): 098701. DOI: 10.1088/1674-1056/ac4a69

Transmembrane transport of multicomponent liposome-nanoparticles into giant vesicles

Hui-Fang Wang(王慧芳), Chun-Rong Li(李春蓉), Min-Na Sun(孙敏娜), Jun-Xing Pan(潘俊星), and Jin-Jun Zhang(张进军)
Chin. Phys. B, 2022, 31 (**4**): 048703. DOI: 10.1088/1674-1056/ac380f

Coarse-grained simulations on interactions between spectrins and phase-separated lipid bilayers

Xuegui Lin(林雪桂), Xiaojie Chen(陈晓洁), and Qing Liang(梁清)
Chin. Phys. B, 2021, 30 (**6**): 068701. DOI: 10.1088/1674-1056/abf129

Probing conformational change of T7 RNA polymerase and DNA complex by solid-state nanopores

Xin Tong(童鑫), Rui Hu(胡蕊), Xiaoqing Li(李晓晴), Qing Zhao(赵清)
Chin. Phys. B, 2018, 27 (**11**): 118705. DOI: 10.1088/1674-1056/27/11/118705

Enhanced effect of dimension of receptor-ligand complex and depletion effect on receptor-mediated endocytosis of nanoparticles

Ye Liu(刘野), Qingqing Gao(高庆庆), Yijun Liu(刘益军), Chuang Zhao(赵闯), Zongliang Mao(毛宗良), Lin Hu(胡林), Yanhui Liu(刘艳辉)
Chin. Phys. B, 2017, 26 (**12**): 128704. DOI: 10.1088/1674-1056/26/12/128704

SPECIAL TOPIC — Celebrating the 100th Anniversary of Physics Discipline of Xiamen University

Pressure-driven membrane inflation through nanopores on the cell wall

Qi Zhong(钟祺)[1], Chen-Xu Wu(吴晨旭)[1,2], and Rui Ma(马锐)[1,2,†]

[1] *Department of Physics, College of Physical Science and Technology, Xiamen University, Xiamen* 361005, *China*
[2] *Fujian Provincial Key Laboratory for Soft Functional Materials Research, Research Institute for Biomimetics and Soft Matter, Xiamen University, Xiamen* 361005, *China*

(Received 19 February 2023; revised manuscript received 17 April 2023; accepted manuscript online 23 May 2023)

Walled cells, such as in plants and fungi, compose an important part of the model systems in biology. The cell wall primarily prevents the cell from over-expansion when exposed to water, and is a porous material distributed with nanosized pores on it. In this paper, we study the deformation of a membrane patch by an osmotic pressure through a nanopore on the cell wall. We find that there exists a critical pore size or a critical pressure beyond which the membrane cannot stand against the pressure and would inflate out through the pore and further expand. The critical pore size scales linearly with the membrane tension and quadratically with the spontaneous curvature. The critical pressure is inversely proportional to the pore radius. Our results also show that the fluid membrane expansion by pressure is mechanically different from the solid balloon expansion, and predict that the bending rigidity of the membrane in walled cells should be much larger than that of the mammalian cells so as to prevent membrane inflation through the pores on the cell wall.

Keywords: membrane mechanics, endocytosis, osmotic pressure, nanopores

PACS: 87.16.D–, 87.15.La **DOI:** 10.1088/1674-1056/acd7cc

1. Introduction

The cell wall is a structure that surrounds the cells of many organisms, including plants, fungi, bacteria, and some protists.[1–4] It is a rigid layer that provides support, protection, and shape to the cell. In plants, the cell wall is composed primarily of cellulose, a polysaccharide made up of glucose units.[5] The cell wall of fungi is composed of chitin, a polymer of N-acetylglucosamine.[6,7] Bacterial cell walls are made up of peptidoglycan, a polymer of amino sugars and amino acids.[8,9] The cell wall plays an important role in maintaining the integrity of the cell and protecting it from mechanical stress, osmotic pressure, and other environmental factors.

Basically, the cell wall is a porous structure that allows for the exchange of materials between the cell and its environment. The size and shape of the pores in the cell wall can vary depending on the type of cells and the function of the wall. For example, in the primary cell wall of plant cells, the size of the pores can range from 10–20 nanometers to several micrometers in diameter, with the largest pores often found at the corners where adjacent cells meet.[10,11] In fungal cell walls, the size of the pores can also vary, but is typically at an order of a few tens of nanometers.[12,13]

Walled cells generally have a high osmotic pressure that allows them to grow and survive in the environment.[14–19] The osmotic pressure pushes the plasma membrane against the cell wall, thus preventing some important biological processes from happening. In particular, endocytosis which involves the internalization of a small patch of plasma membrane is hindered by the osmotic pressure.[20] In fission yeast cells, the turgor pressure is estimated to be 0.85 ± 0.15 MPa by measuring the growth curve of a mutant yeast cell against a PDMS chamber.[21,22] In another experiment which compares the geometry of a fission yeast cell upon osmolarity change, it is estimated that the turgor pressure is up to 1.5 ± 0.2 MPa.[14] Based on a similar osmolarity variation method, the value of turgor pressure is estimated to be 0.6 ± 0.2 MPa in budding yeast.[23] In general, the turgor pressures in yeast cells have an order of magnitude of 0.1–1 MPa.

Membrane deformation caused by osmotic pressure has been studied both in theory[24,25] and in experiments.[26–28] Different from the cell membranes which exhibit a fluid behavior, the membranes studied in the experiments are typically composed of crosslinked polymer networks which provide a relatively solid structure, and therefore the membranes are treated as an elastic shell which has an intrinsic shape. A spherical shell has been shown to undergo a buckling transition upon osmolarity change.[24,25] The deflection of a flat shell as a function of the external pressure has been exploited to measure the elasticity of the shell and quantify the osmotic pressure.[28] However, the deflection of a fluid membrane, which does not have an intrinsic shape, by osmotic pressure has been rarely studied.

In this work, we study the deformation of a fluid membrane through a nanopore on the cell wall by the osmotic pres-

†Corresponding author. E-mail: ruima@xmu.edu.cn

© 2023 Chinese Physical Society and IOP Publishing Ltd

sure with the Helfrich model. We find that when the pore is small, the membrane assumes a dimple shape to resist the osmotic pressure. When gradually increasing the pore size beyond a critical value, the membrane cannot stand against the pressure anymore and would inflate out through the pore and further expand. We systematically study how the critical pore size $R_{\rm crit}$ depends on the membrane properties and find that $R_{\rm crit}$ scales linearly with the membrane tension and quadratically with the spontaneous curvature. Furthermore, we show that the deflection of a flat fluid membrane by osmotic pressure is different from a solid one in terms of their p–V curve. When gradually increasing the osmotic pressure, there exists a critical pressure $p_{\rm crit}$ beyond which the membrane would inflate out through the pore and further expand. Our results suggest that the membrane bending rigidity in walled cells should be larger than that in mammalian cells so as to prevent the cell from inflation through the nanopores present on the cell wall.

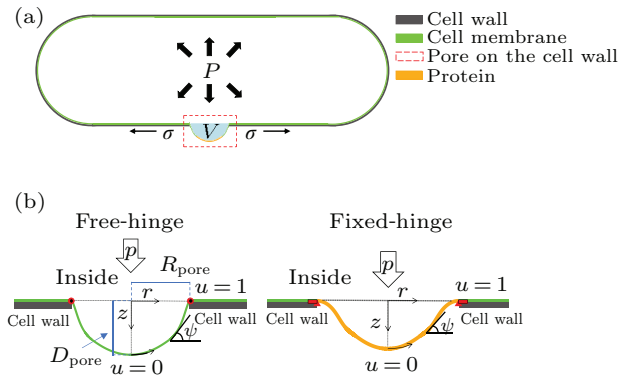


Fig. 1. Schematic illustration of a typical yeast cell and the model. (a) Illustration of the typical morphology of a fission yeast cell. A nanopore (red frame) is present on the cell wall (gray) and the membrane (green) is pushed outwards by the osmotic pressure p. The size of the nanopore is exaggerated for the purpose of illustration only. (b) Illustration of the membrane models. The membrane shape is assumed to be axisymmetric with respect to the z-axis, and parameterized by its meridinal coordinates $[r(u),z(u)]$ with $u=0$ labeling the membrane tip and $u=1$ labeling the membrane edge. Two types of boundary conditions (BCs) are considered, namely, the free-hinge BC (left) in which the membrane is allowed to freely rotate at the pore edge and the fixed-hinge BC (right) in which the membrane angle is fixed. The bare membrane (green) is assumed to have a zero spontaneous curvature and the effect of proteins (orange) coated on the membrane is assumed to generate a nonzero spontaneous curvature of the membrane.

2. Methods

2.1. Model

Theoretical study of fluid membranes can be roughly divided into two categories, one utilizing the molecular dynamics (MD) simulations in which the membrane is explicitly treated as a collection of lipid molecules, the other taking advantage of the continuum mechanics which treats the membrane as a smooth surface. The MD simulations are widely used to study the interaction of lipid molecules and proteins in the membrane.[29–32] However, when studying the large scale membrane deformation, MD simulations are computationally too intensive and expensive. In this paper, we adopt the classical Helfrich theory of membrane which is a continuum model and has broad applications in studying the large scale deformation of membrane.[33–39]

We consider a walled cell with a high osmotic pressure p that pushes the cell membrane against the cell wall. A nanopore with a radius of $R_{\rm pore}$ is present on the cell wall (Fig. 1(b)) which has a much larger Young's modulus than the osmotic pressure and a much smaller curvature than $1/R_{\rm pore}$.[40–44] The cell wall is therefore modeled as a rigid and flat substrate. As a result of the osmotic pressure, the flat membrane is deflected to a depth of $D_{\rm pore}$ as illustrated in Fig. 1(b). We assume the deformation of the membrane at the pore is axisymmetric, and parameterized with its meridional coordinates $[r(u),z(u)]$, where $u\in[0,1]$ is the rescaled arclength. The point at $u=0$ labels the membrane tip and the points at $u=1$ label the membrane edge (Fig. 1(b)). The coordinates satisfy the geometric relations

$$r'=h\cos\psi,\quad z'=-h\sin\psi. \tag{1}$$

Hereafter, we use f' to denote the derivative of an arbitrary function f with respect to u. The angle $\psi(u)$ spans between the tangential direction and the horizontal direction. The constant h is essentially the total arclength of the membrane profile and is to be solved with the shape equations. The total energy of the membrane reads

$$G=\frac{\kappa}{2}\int(c_1+c_2-c_0)^2\,{\rm d}A+\sigma A+pV, \tag{2}$$

where the first term is the classical Helfrich bending energy with κ denoting the bending rigidity of the membrane, $c_1=\psi'/h$ and $c_2=\sin\psi/r$ denoting the two principal curvatures of the membrane surface, c_0 denoting the spontaneous curvature induced by curvature-generating proteins coated on the membrane.[36,37,45–48] In the absence of proteins, the spontaneous curvature of the bare membrane is assumed to vanish, i.e., $c_0=0$. The second term in Eq. (2) is the surface tension energy with A denoting the surface area of the deformed membrane, and σ denoting the membrane tension at the edge of the pore. The third term describes the effect of the osmotic pressure with V being the increased volume of the membrane due to inflation, and p denoting the osmotic pressure (Fig. 1(a)). We choose the convention such that a positive p pushes the membrane downward which results in a negative volume V. Due to the rotational symmetry of the membrane shape about the z axis, the total energy of the membrane in Eq. (2) can be expressed as a functional of the shape variables

$$\begin{aligned}&G[\psi,\psi',r,r',z,z',h,\gamma,\eta]\\&=2\pi\int_0^1 L[\psi,\psi',r,r',z,z',h,\gamma,\eta]\,{\rm d}u.\end{aligned} \tag{3}$$

Here γ and η are Lagrangian multipliers that enforce the geometric relations in Eq. (1). The shape equations of the membrane are obtained by applying variations of the free energy G with respect to all the shape variables.[38,39] The variation δG contains both bulk terms, e.g., $[\partial L/\partial\psi - \mathrm{d}(\partial L/\partial\psi')/\mathrm{d}u]\,\delta\psi$, and boundary terms, e.g., $(\partial L/\partial\psi')\delta\psi|_{u=0}^{u=1}$. We obtain the shape equations by having the bulk terms be zero. In addition, proper boundary conditions (BCs) at the membrane tip $u = 0$ and at the pore edge $u = 1$ need to be specified, which can be achieved by setting the boundary terms in δG to be zero. There are two types of BCs, the free-hinge BC in which the membrane angle ψ is allowed to freely rotate, and the fixed-hinge BC in which the membrane angle ψ is fixed to be 0 (Fig. 1(b)). They correspond to either $\partial L/\partial\psi' = 0$ or $\delta\psi = 0$ in the boundary term. The detailed derivation of the shape equations and the BCs is provided in Appendices A and B. We find that the two BCs only lead to qualitative differences in the membrane deformations (see the discussion), and therefore only present results for the free-hinge BC if otherwise mentioned.

We numerically solve the shape equations with the bvp4c solver in MATLAB, which is designed for solving boundary value problems (BVPs) of ordinary differential equations.

3. Results

3.1. Critical pore size scales linearly with the membrane tension and quadratically with the spontaneous curvature

Firstly, we fix the osmotic pressure p and study how the membrane is deformed when gradually increasing the pore radius R_{pore}. The osmotic pressure p and the membrane bending rigidity κ define a characteristic length $R_p = [\kappa/(2p)]^{1/3}$, which is used to rescale the length, and nondimensionalizes all the other parameters. In particular, the rescaled pressure $\bar{p} = pR_p^3/\kappa = 0.5$ is a constant. The other nondimensionalized parameters include the rescaled tension $\bar{\sigma} = \sigma R_p^2/\kappa$, the rescaled spontaneous curvature $\bar{c}_0 = c_0 R_p$ and the rescaled free energy $\bar{G} = G/2\pi\kappa$. Hereafter, we always use $\bar{x}$ to indicate the rescaled (dimensionless) x.

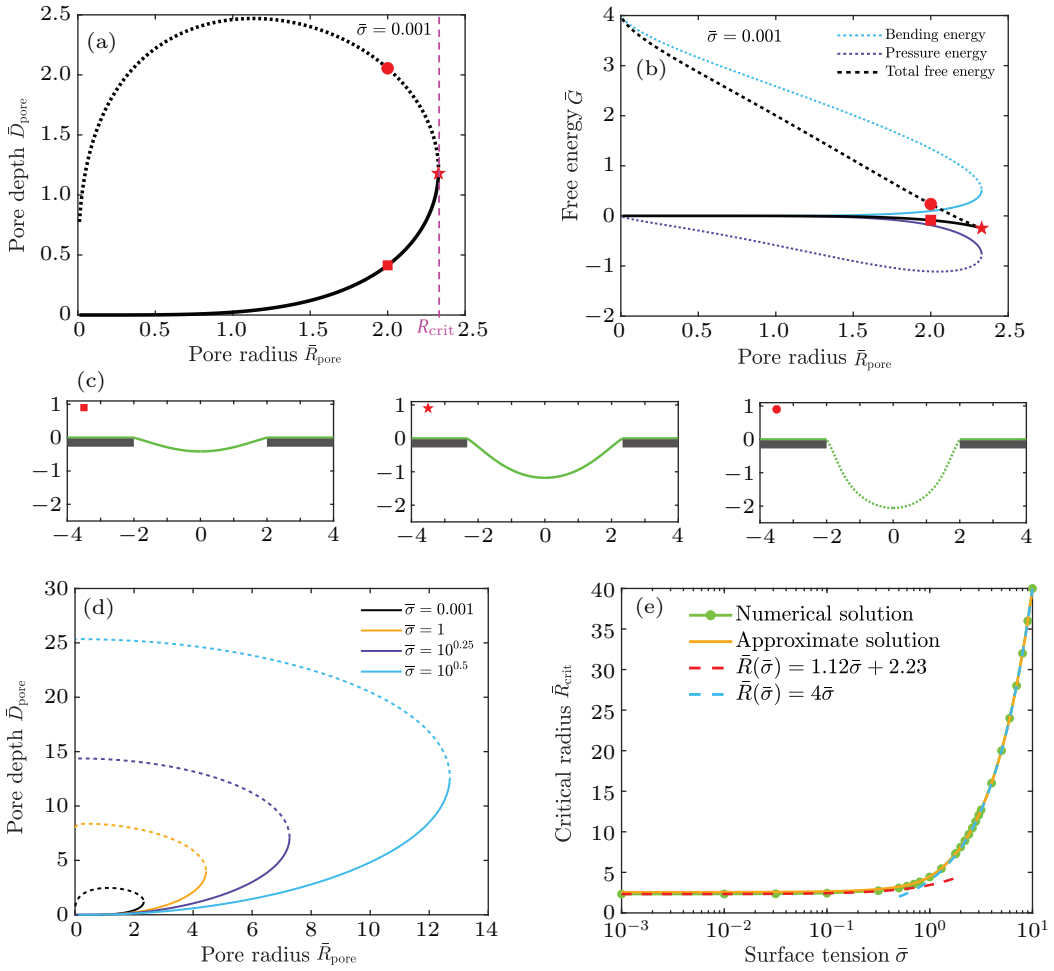


Fig. 2. Effect of the surface tension on the critical radius of an uncoated membrane. (a) D_{pore} vs. R_{pore} curve of membrane deformations for an uncoated membrane. The critical pore size, beyond which no solutions are found, is indicated by a pentagon. (b) The free energy curve of the corresponding membrane deformations in (a). The solid curve indicates a stable state, and the dashed line indicates a metastable state. (c) Illustration of the membrane shapes indicated by the corresponding symbols on the D_{pore} vs. R_{pore} curve. (d) D_{pore} vs. R_{pore} curves are shown for different membrane tensions $\bar{\sigma}$. (e) The critical pore size as a function of the surface tension $\bar{\sigma}$. The green curve represents the numerical solution. The dashed red curve and the dashed cyan curve represent the linear fitting between the critical radius R_{crit} and the membrane tension $\bar{\sigma}$ at small $\bar{\sigma}$ and large $\bar{\sigma}$, respectively.

We first consider a bare membrane, which is assumed to have a zero spontaneous curvature $\bar{c}_0 = 0$. As a result of the osmotic pressure, the membrane is pushed downwards to a depth of $\bar{D}_{\text{pore}}$ through the pore with a radius of $\bar{R}_{\text{pore}}$. It is found in the $\bar{D}_{\text{pore}}$–$\bar{R}_{\text{pore}}$ curve that a single value of the pore radius $\bar{R}_{\text{pore}}$ corresponds to two membrane shapes (squares and circles in Fig. 2(c)), one with a shallow depth and the other with a deep one. By comparing the total energies of the two shapes (Fig. 2(b)), we see that the energy of the shallow solution is much lower than that of the deep one, indicating an energetically more favorable state of the membrane. For the shallowly deflected membrane (Fig. 2(c), left), the depth of the membrane is pushed further down by the pressure as the pore size is enlarged (solid lines in Fig. 2(a)), while for the deeply deflected membrane (Fig. 2(c), right), the depth of the membrane shows a nonmonotonic relation with the pore radius (dashed lines in Fig. 2(a)). We define the critical radius R_{crit} as the maximum value of the pore radii in the D_{pore}–R_{pore} curve, as indicated by the asterisk in Fig. 2(a). If the pore radius is beyond R_{crit}, the osmotic pressure is too strong for any membrane shape to sustain the pressure, and the membrane would continuously inflate out of the pore and expand over time.

We then plot the $\bar{D}_{\text{pore}}$ vs. $\bar{R}_{\text{pore}}$ curves for different membrane tensions $\bar{\sigma}$ (Fig. 2(b)). The critical pore size $\bar{R}_{\text{crit}}$ is found to strongly depend on the membrane tension $\bar{\sigma}$. For $\bar{\sigma} < 0.1$, the critical radius can be nicely fitted by the expression $\bar{R}_{\text{crit}} = 1.12\bar{\sigma} + 2.23$ (Fig. 2(e), red dashed curve). Beyond $\bar{\sigma} = 1$, the critical radius is found to scale linearly with the membrane tension and can be well fitted by a simple relation $\bar{R}_{\text{crit}} = 4\bar{\sigma}$ (Fig. 2(e), green dashed curve).

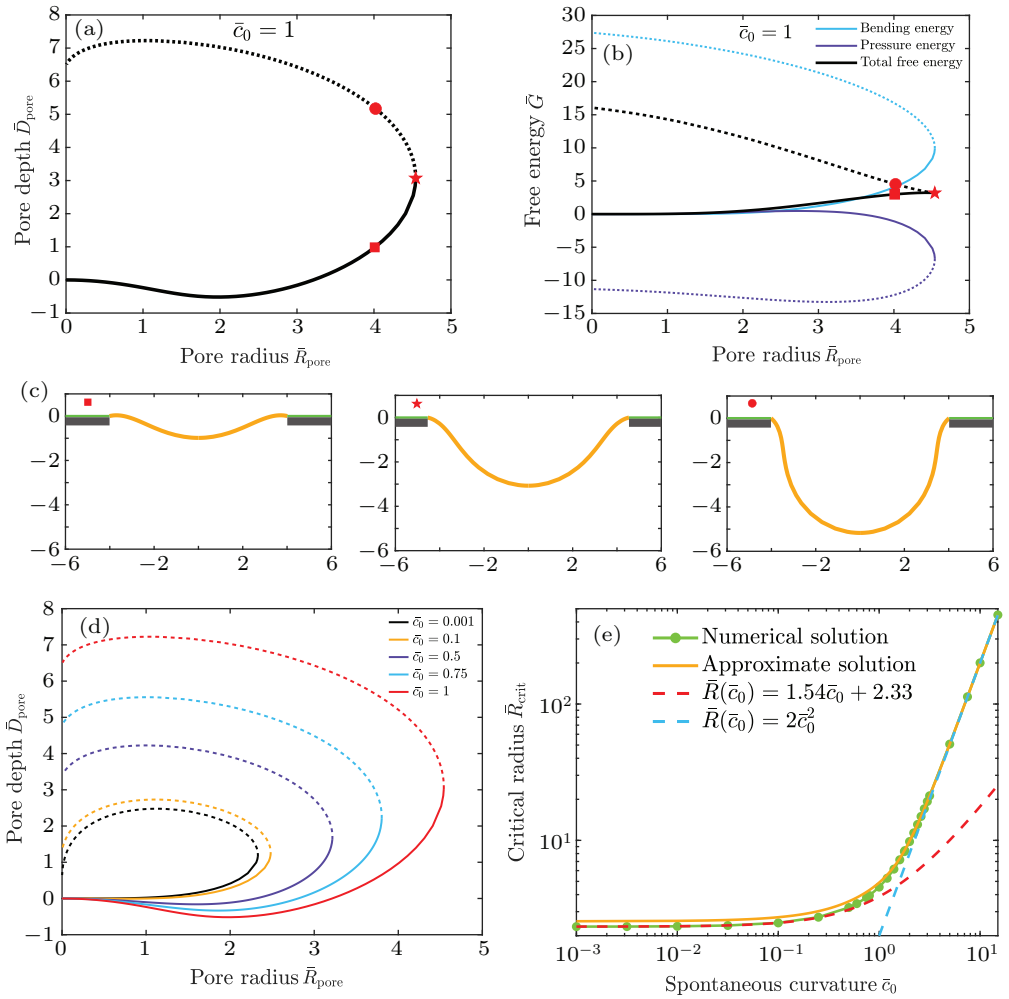


Fig. 3. Effect of the spontaneous curvature on the critical radius of a totally coated membrane. (a) D_{pore} vs. R_{pore} curve of membrane deformations for a totally coated membrane with spontaneous curvature $\bar{c}_0 = 1$. The critical pore size is indicated by a pentagon. (b) The free energy curve of the corresponding membrane deformations in (a). The solid line indicates a stable state, and the dashed line indicates a metastable state. (c) Illustration of the membrane shapes indicated by the corresponding symbols on the D_{pore} vs. R_{pore} curve. (d) D_{pore} vs. R_{pore} curves are shown for different spontaneous curvatures $\bar{c}_0$. (e) The critical pore size as a function of the spontaneous curvature $\bar{c}_0$. The green curve represents the numerical solution. The red dashed curve represents the linear fitting of the critical radius R_{crit} at small spontaneous curvature $\bar{c}_0$ and the cyan dashed curve represents the quadratic fitting at large $\bar{c}_0$.

We next consider a protein-coated membrane and study the effect of spontaneous curvature c_0 induced by the proteins on the membrane deformation, particularly on the critical pore radius. The membrane tension is fixed to a small value of $\bar{\sigma} = 0.001$. The $\bar{D}_{\text{pore}}$–$\bar{R}_{\text{pore}}$ curve for a coated membrane with positive $\bar{c}_0$ shows a similar trend with that of the

uncoated membrane, i.e., a single pore radius corresponding to two solutions, one with a shallow depth and a lower energy and the other with a higher depth and a higher energy (Figs. 3(a) and 3(b)). However, solutions with negative depth appear for small pore radii in the lower energy branch due to the positive spontaneous curvature c_0 that tends to bend the membrane upward against the osmotic pressure (Fig. 3(a)). When the pore radius becomes large, the spontaneous curvature c_0 cannot resist the osmotic pressure anymore and the membrane is pushed downward by the pressure (Fig. 3(c)). The $D_{\rm pore}$–$R_{\rm pore}$ curves for different spontaneous curvatures c_0 are shown in Fig. 3(d). The numerical solution for the critical radius is found to increase linearly with the spontaneous curvature as $R_{\rm crit} = 1.54\bar{c}_0 + 2.33$ when $\bar{c}_0 < 0.1$ (Fig. 3(e), dashed red curve) and scales to the square of the spontaneous curvature $R_{\rm crit} = 2\bar{c}_0^2$ for $\bar{c}_0 > 1$ (Fig. 3(e), dashed cyan curve).

3.2. Critical pressure is inversely proportional to the pore radius

We now fix the pore radius and study how an uncoated membrane is deformed by gradually increasing the osmotic pressure p. In this case, the membrane tension σ and the membrane bending rigidity κ define a characteristic length $R_\sigma = [\kappa/(2\sigma)]^{1/2}$, which is used to rescale the length, and nondimensionalizes all the other parameters. In particular, the membrane tension can be rescaled to a constant $\bar{\sigma} = \sigma R_\sigma^2/\kappa = 0.5$. The rescaled osmotic pressure is $\bar{p} = pR_\sigma^3/\kappa$.

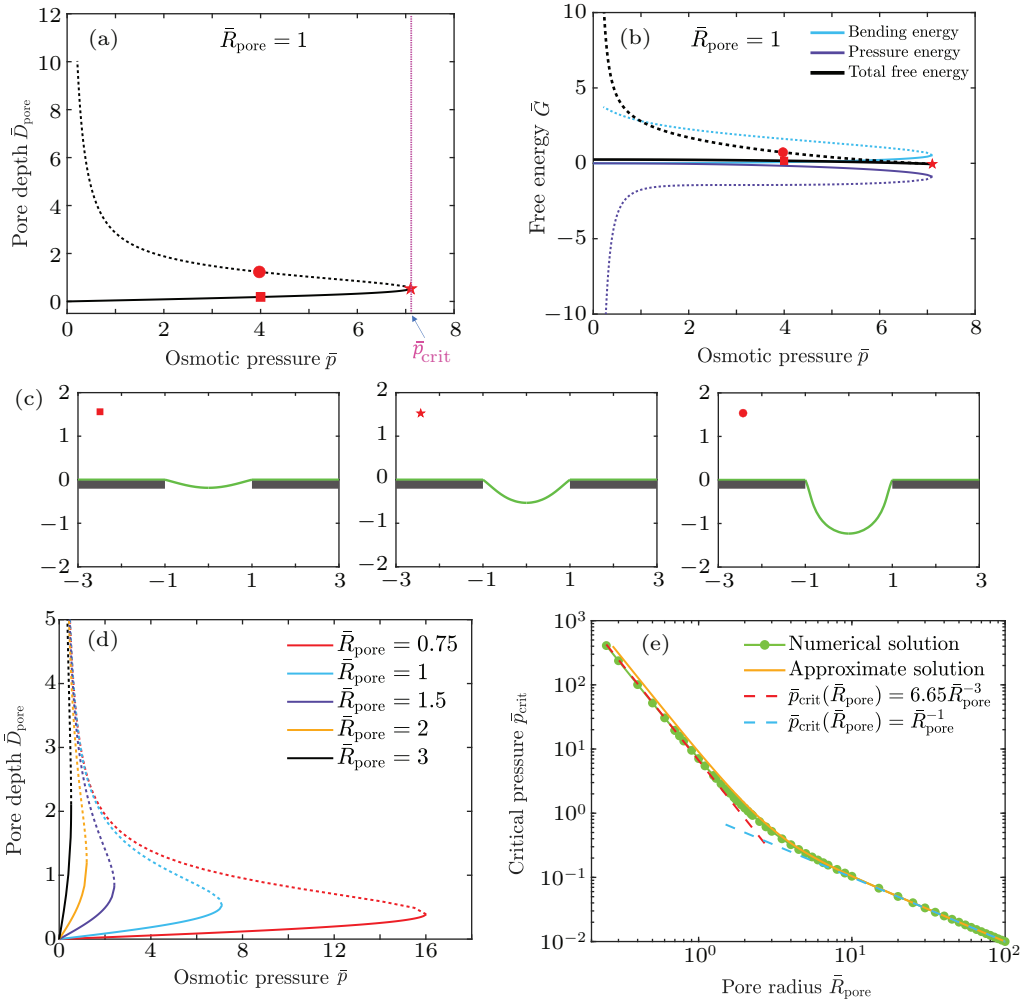


Fig. 4. Effect of the osmotic pressure on the membrane deformation for an uncoated membrane. (a) $D_{\rm pore}$ vs. $\bar{p}$ curve of membrane deformations for an uncoated membrane. The pore size is fixed at $\bar{R}_{\rm pore} = 1$. The critical osmotic pressure is indicated by a pentagon. (b) The free energy curve of the corresponding membrane deformations in (a). The solid curve indicates a stable state and the dashed curve indicates a metastable state. (c) Illustration of the membrane shapes indicated by the corresponding symbols on the $D_{\rm pore}$ vs. $\bar{p}$ curve. (d) $D_{\rm pore}$ vs. $\bar{p}$ curves are shown for different pore size $\bar{R}_{\rm pore}$. (e) The critical pressure as a function of the pore size $\bar{R}_{\rm pore}$. The green dotted curve represents the numerical solutions. The red dashed curve represents a power law fitting of $\bar{p}_{\rm crit} \propto (\bar{R}_{\rm pore})^{-3}$ at small pore radius $\bar{R}_{\rm pore}$. The cyan dashed curve represents a power law fitting of $\bar{p}_{\rm crit} \propto (\bar{R}_{\rm pore})^{-1}$ at large $\bar{R}_{\rm pore}$.

As a result of the osmotic pressure $\bar{p}$, the membrane is pushed downwards to a depth of $\bar{D}_{\rm pore}$. A typical $\bar{D}_{\rm pore}$ vs. $\bar{p}$ curve is shown in Fig. 4(a). A single osmotic pressure $\bar{p}$ has two corresponding depths on the curve, with the shallow one having a lower energy and the deep one having a higher energy (Figs. 4(b) and 4(c)). Note that for small osmotic pressure p, the high energy branch can have a very large depth (Fig. 4(a), dashed line). This is similar to the p–V curve of an inflating balloon.[49–53] We define the critical pressure $\bar{p}_{\rm crit}$ as the maximum value of the osmotic pressure $\bar{p}$ in the $\bar{D}_{\rm pore}$ vs. $\bar{p}$ curve,

as indicated by the asterisk in Fig. 4(a). When the osmotic pressure is beyond $\bar{p}_{\rm crit}$, no solutions are found. It implies that the osmotic pressure is too strong for any membrane shape to sustain. The membrane would inflate out of the pore and expand. The critical pressure $\bar{p}_{\rm crit}$ is found to decrease with the pore radius $\bar{R}_{\rm pore}$ (Fig. 4(d)). For small $\bar{R}_{\rm pore}$, the critical pressure is inversely proportional to $(\bar{R}_{\rm pore})^3$ (Fig. 4(d), red dashed curve). For large $\bar{R}_{\rm pore}$, it can be well fitted with the equation $\bar{p}_{\rm crit} = 1/\bar{R}_{\rm pore}$ (Fig. 4(d), cyan dashed curve).

3.3. Spherical cap approximation

So far, we have fixed the pressure p and calculated the critical radius $R_{\rm crit}$ as a function of the membrane tension σ and the spontaneous curvature c_0. The scaling behaviors $\bar{R}_{\rm crit} = 4\bar{\sigma}$ and $\bar{R}_{\rm crit} = 2(\bar{c}_0)^2$ have been shown to hold when the corresponding variables are large (cyan dashed lines in Figs. 2(e) and 3(e)). We have also fixed the membrane tension σ and calculated the critical pressure $p_{\rm crit}$ as a function of the pore radius $R_{\rm pore}$. It is found that the scaling behavior of $\bar{p}_{\rm crit} = (\bar{R}_{\rm pore})^{-1}$ holds for large $\bar{R}_{\rm pore}$ (cyan dashed lines in Fig. 4(e)). To further reveal the physics behind the numerical calculation, we adopt an ansatz in which the shape of the membrane is assumed as a spherical cap,[54] i.e.,

$$r(u) = R_0 \sin u\alpha, \quad z(u) = R_0(\cos u\alpha - \cos\alpha), \tag{4}$$

where R_0 is the radius of the sphere, and α is the half angle spanned by the spherical cap, as illustrated in Figs. 5(a)–5(c). The pore size $R_{\rm pore}$ sets a constraint on R_0 and α

$$R_0 \sin\alpha = R_{\rm pore}. \tag{5}$$

For spherical caps bending downward (upward), we adopt the convention $R_0 < 0$ and $\alpha < 0$ ($R_0 > 0$ and $\alpha > 0$). The area A and volume V of the spherical cap read

$$\begin{aligned} A &= R_0^2(1-\cos\alpha), \\ V &= \frac{2}{3}R_0^3(2+\cos\alpha)\sin^4\frac{\alpha}{2}. \end{aligned} \tag{6}$$

The principal curvatures $c_1 = c_2 = 1/R_0$. The total free energy then can be expressed as

$$G(\alpha, R_0) = \left[\frac{\kappa}{2}\left(\frac{2}{R_0} - c_0\right)^2 + \sigma\right]A + pV. \tag{7}$$

If we replace R_0 with $R_{\rm pore}/\sin\alpha$ in Eq. (7) via the relation (5), the free energy $G(\alpha, R_0)$ becomes a function of $G(\alpha, R_{\rm pore})$. We find that when $R_{\rm pore}$ is small, $G(\alpha, R_{\rm pore})$ as a function of α is non-monotonic, with a local minimum and a local maximum respectively (Fig. 5(d), square and circle). The two extremums actually correspond to the two numerical solutions found for a single pore radius $R_{\rm pore}$ in Fig. 2(a), with one having a deeply deflected membrane shape and the other being shallowly deflected (Figs. 5(a) and 5(b)). When $R_{\rm pore}$ is large, $G(\alpha, R_{\rm pore})$ becomes monotonic with respect to α and its minimum is located at $\alpha = -\pi$ (Fig. 5(f)), which corresponds to a spherical cap with an infinite radius $R_0 = -\infty$ due to the relation (5). The transition from a nonmonotonic function to a monotonic function happens at a critical radius $R_{\rm crit}$ such that the local minimum and the local maximum merge into a single one. Mathematically, this implies the equations

$$\frac{\partial G}{\partial \alpha}(\alpha_{\rm crit}, R_{\rm crit}) = 0, \quad \frac{\partial^2 G}{\partial \alpha^2}(\alpha_{\rm crit}, R_{\rm crit}) = 0. \tag{8}$$

We numerically solve Eq. (8) to obtain the critical radius $R_{\rm crit}$ and the corresponding angle $a_{\rm crit}$ under the spherical cap approximation. The approximated solutions are in good agreement with the exact numerical solutions (orange curves in Figs. 2 and 3). Furthermore, we find that for a fixed pressure p, when the membrane tension σ is large or the spontaneous curvature c_0 is large, the critical angle $\alpha_{\rm crit} \approx -\pi/2$, which means the membrane assumes a hemispherical shape. If we substitute $\alpha = -\pi/2$ into the equation $\partial G/\partial\alpha = 0$, we have the equation

$$p - \left(\frac{2}{R_{\rm crit}} + c_0\right)^2 \frac{\kappa}{R_{\rm crit}} - 2\frac{\sigma}{R_{\rm crit}} = 0, \tag{9}$$

which is essentially the force balance equation in the normal direction for a hemisphere. With the nondimensionalized quantities $\bar{R}_{\rm crit} = R_{\rm crit}/R_p$ and $\bar{\sigma} = R_p^2\sigma/\kappa$, Eq. (9) can be rewritten as

$$\frac{1}{2}(\bar{R}_{\rm crit})^3 - (2 + \bar{c}_0\bar{R}_{\rm crit})^2 - 2(\bar{R}_{\rm crit})^2\bar{\sigma} = 0. \tag{10}$$

In the case of $\bar{c}_0 = 0$, we neglect the second term in Eq. (10) and get the analytical result

$$\bar{R}_{\rm crit} = 4\bar{\sigma} \tag{11}$$

for large $\bar{\sigma}$, which agrees exactly with the numerical solutions in Fig. 2(e). In the case of a large spontaneous curvature $\bar{c}_0$ and small membrane tension $\bar{\sigma}$, we neglect the third term in Eq. (10) and take only the quadratic term of $\bar{c}_0$ in the second term to obtain the analytical result

$$\bar{R}_{\rm crit} = 2(\bar{c}_0)^2, \tag{12}$$

which agrees exactly with the numerical solutions in Fig. 3(e).

When considering the critical pressure $p_{\rm crit}$ under the fixed membrane tension σ, we use the the characteristic length R_σ to nondimensionalize the quantities and Eq. (10) can be rewritten as

$$\bar{p}_{\rm crit}(\bar{R}_{\rm pore})^3 - (2 + \bar{c}_0\bar{R}_{\rm pore})^2 - (\bar{R}_{\rm pore})^2 = 0. \tag{13}$$

In the case of $\bar{c}_0 = 0$ and large pore radius $\bar{R}_{\rm pore}$, we neglect the second term in Eq. (13) and obtain the analytical result

$$\bar{p}_{\rm crit} = \frac{1}{\bar{R}_{\rm pore}}, \tag{14}$$

which agrees exactly with the numerical solutions in Fig. 4(e).

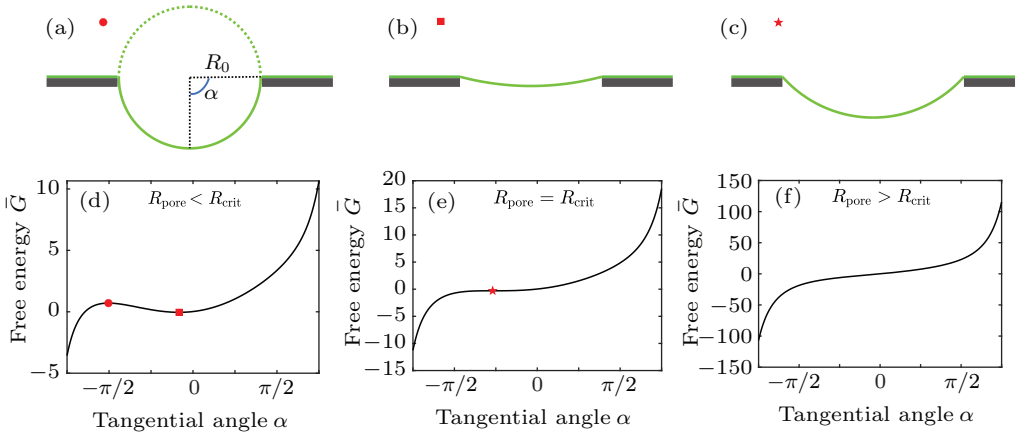


Fig. 5. Membrane shapes and free energy under the spherical cap approximation. (a)–(c) Different membrane shapes under the spherical cap approximation. The spherical cap has a radius of R_0 and spans an angle 2α. (d)–(f) The free energy as a function of the angle α for pore radius $R_{\rm pore} < R_{\rm crit}$ in (d), $R_{\rm pore} = R_{\rm crit}$ in (e), and $R_{\rm pore} > R_{\rm crit}$ in (f). The circle and the square in (d) indicate the local energy minimum and maximum, respectively, and the corresponding membrane shapes are illustrated in (a) and (b). The pentagon in (e) indicates the critical point of $\partial G/\partial\alpha = 0$ and $\partial^2 G/\partial\alpha^2 = 0$ and the corresponding membrane shape is illustrated in (c).

4. Discussion

4.1. Physical interpretation of the critical radius and critical pressure

We have shown that if a nanopore is present on the cell wall and the pore radius is small, the membrane is able to resist the osmotic pressure by assuming a curved shape. If the pore radius is beyond a critical value $R_{\rm crit}$, no membrane shapes are able to sustain the osmotic pressure and the membrane would inflate out and further expand. In fact, this is a result of the competition between the elastic energy (including both the bending energy and the membrane tension energy) which tends to flatten the membrane, and the pressure energy which tends to deflect the membrane. When the membrane is pushed downward by the osmotic pressure from the flat shape, its elastic energy is increased while the pressure energy pV is reduced (p is positive and V is negative). If the pore radius is small, there exists a state in which the two energy contributions balance each other and the membrane in this state is shallowly deflected. Further deflection of the membrane leads to more increased elastic energy than the reduced pressure energy, and therefore this state is stable (see energy decomposition in Figs. 2(b) and 3(b)). On the other hand, if the pore radius is large, as the membrane expands larger and larger through the pore, the reduced pressure energy always dominates over the increased elastic energy such that the total free energy always decreases. The membrane would continuously inflate out of the pore and expand to an infinitely large bulge.

4.2. The critical pore size is about 10 nm given the typical parameters of the membrane

As an application of the theory, we estimate the critical pore size based on the typical values of the membrane properties listed in Table 1. In Fig. 6, we show the critical pore size as a function of the model parameters, which include the bending rigidity κ, the membrane tension σ, the osmotic pressure p, and the spontaneous curvature c_0. We fix three of them to the typical values (listed on the top of each panel in Fig. 6), and vary the fourth one to see how it impacts the critical pore size $R_{\rm crit}$ which is calculated numerically with the MATLAB solver bvp4c explained in Appendix C. We show results for both the free-hinge BC and the fixed-hinge BC. In general, $R_{\rm crit}$ is smaller under the free-hinge BC than that under the fixed hinge BC. The bending rigidity κ of a lipid membrane is typically in the range of 5–50 kT. If the osmotic pressure is 1 MPa, the corresponding critical radius falls in the range of 5–15 nm (Fig. 6(b)). As we have pointed out in the introduction, the typical pore size of the cell wall is about tens of nanometers,[10–13] which overlaps with the range of 5–15 nm. Furthermore, we find that if the bending rigidity $\kappa = 20\ kT$, neither increasing the surface tension to as high as the upper bound 0.3 pN/nm listed in Table 1, nor increasing the spontaneous curvature up to 0.2 nm^{-1} would not dramatically raise up the critical radius (Figs. 6(a) and 6(d)). The above calculation therefore implies that the bending rigidity of the walled cells must be in the order of 1000 kT, which results in a critical radius of 30–40 nm (Fig. 6(b)). This is plausible based on the experimental evidence that the membrane is surrounded with an actin meshwork in yeast cells,[55–57] which is able to effectively increase the bending rigidity of the membrane. Furthermore, proteins on the membrane also help to increase the bending rigidity.

Table 1. Typical values of the membrane properties.

Parameters	Values	Unit	References
κ	5–50	kT	[58–60]
σ	0.01–0.3	pN/nm	[61–64]
p	0.5–3	MPa	[14–19]
c_0	0.01–0.2	nm^{-1}	[65–67]

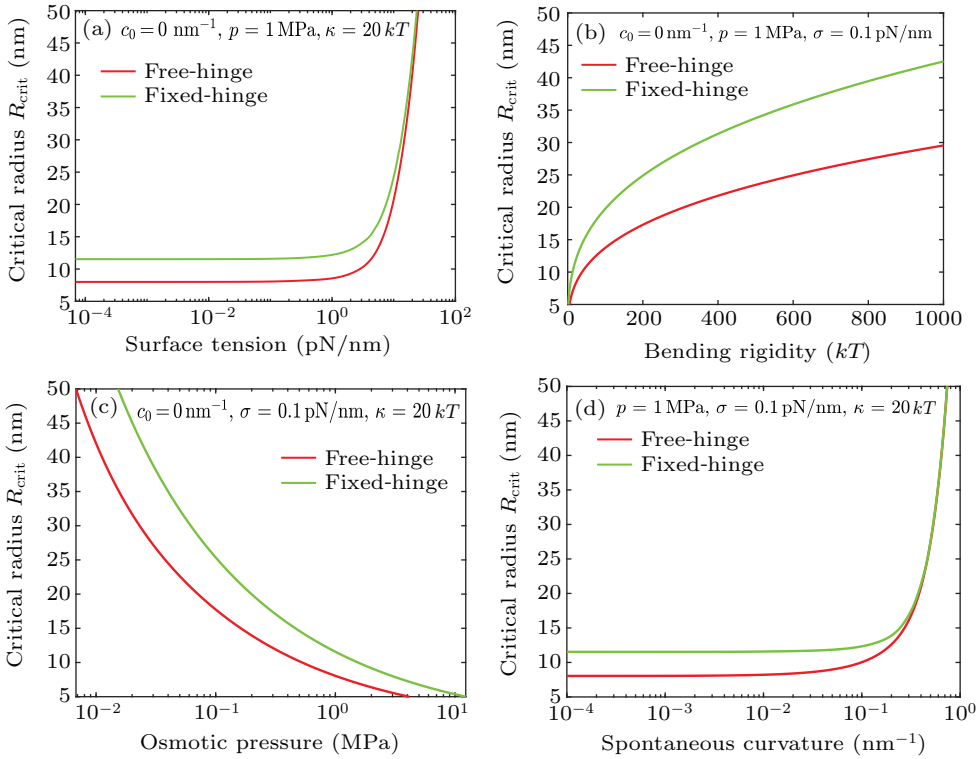


Fig. 6. Dependence of the critical pore size on the model parameters. The typical values of the fixed parameters are listed on top of each panel. The red curve is for the free-hinge BC and the green curve is for the fixed-hinge BC. (a)–(d) The relationship between the critical radius R_{crit} and the surface tension σ, the bending rigidity κ, the osmotic pressure p, and the spontaneous curvature c_0, respectively.

4.3. Liquid membrane versus solid balloon

In Fig. 4, we have presented the results for the membrane deformation when gradually increasing the osmotic pressure. The $\bar{D}_{pore}$ vs. $\bar{p}$ curve is found to be nonmonotonic, which resembles the p–V curve of an inflating balloon.[49–53] In fact, the deflection of a flat membrane made of polymer networks by osmotic pressure has been used to measure the elastic properties of the membrane.[28] However, for the solid balloon, in particular, at very large volume, the p–V curve would increase with the pressure again due to the stretching energy of the rubber that makes up the balloon. In our case, we consider an incompressible liquid membrane and the membrane area increase is due to the lipid flow from the pore edge when the membrane is pushed by the osmotic pressure. The membrane tension σ at the edge is fixed instead of increasing with the depth. Therefore, we can find deep invaginations at very small pressure. However, since the lipid reservoir is finite, the membrane tension cannot be a constant as the membrane inflates out and expands. Studying the effect of the increased membrane tension on the membrane deformation would be our future work.

5. Conclusion

We have studied membrane inflation through a nanopore on the cell wall in the presence of a high osmotic pressure. It is found that there exists a critical value of the pore size R_{crit} beyond which the membrane cannot stand against the osmotic pressure and would inflate out through the pore and keep expansion. The critical pore size R_{crit} scales linearly with the membrane tension σ and quadratically with the spontaneous curvature c_0. In the case of a fixed pore radius, there exists a critical pressure p_{crit} beyond which the membrane would inflate out. The critical pressure p_{crit} scales inversely with the pore radius R_{pore} as $1/R_{pore}$. The boundary conditions at the pore edge also make a quantitative difference. In general, the fixed-hinge BC leads to a larger R_{crit} than the free-hinge BC. Our results also reveal that the inflation of a liquid membrane by pressure behaves differently from that of a solid balloon. In walled cells where the osmotic pressure is high, the membrane should have a much larger bending rigidity ($\sim 1000\,kT$) than that in mammalian cells ($\sim 10\,kT$) to prevent it from inflation through the pores on the cell wall.

Appendix A: Derivation of the membrane shape equations

In order to derive the membrane shape equations, we explicitly express the integrand L in Eq. (3) as

$$L = \frac{1}{2}\kappa\left(\frac{\psi'}{h} + \frac{\sin\psi}{r} - c_0\right)^2 rh + \frac{p}{2}r^2 h\sin\psi + \sigma hr + \gamma(u)(r' - h\cos\psi) + \eta(u)(z' + h\sin\psi). \tag{A1}$$

Here the three terms in the first line describe the energy contribution made by the bending rigidity, the osmotic pressure

and the surface tension, respectively, and the two terms in the second line describe the Lagrangian multiplies $\gamma(u)$ and $\eta(u)$ to enforce the geometric constraints Eq. (1). The variation of the functional G in Eq. (3) reads

$$\begin{aligned}\frac{\delta G}{2\pi} = &\int_0^1 \mathrm{d}u\left[\left(\frac{\partial L}{\partial \psi}-\frac{\mathrm{d}}{\mathrm{d}u}\frac{\partial L}{\partial \psi'}\right)\delta\psi+\left(\frac{\partial L}{\partial r}-\frac{\mathrm{d}}{\mathrm{d}u}\frac{\partial L}{\partial r'}\right)\delta r\right.\\ &\left.+\left(\frac{\partial L}{\partial z}-\frac{\mathrm{d}}{\mathrm{d}u}\frac{\partial L}{\partial z'}\right)\delta z\right]\\ &+\int_0^1 \mathrm{d}u\left[\frac{\partial L}{\partial \gamma}\delta\gamma+\frac{\partial L}{\partial \eta}\delta\eta+\frac{\partial L}{\partial h}\delta h\right]\\ &+\frac{\partial L}{\partial \psi'}\delta\psi\Big|_{u=0}^{u=1}+\frac{\partial L}{\partial r'}\delta r\Big|_{u=0}^{u=1}+\frac{\partial L}{\partial z'}\delta z\Big|_{u=0}^{u=1}. \end{aligned} \tag{A2}$$

The variation contains both the bulk terms (first and second lines) and the boundary terms (third line). By letting the bulk terms equal to zero, we obtain a set of ordinary differential equations, which include a second-order equation

$$\begin{aligned}\psi'' = &\frac{h^2\cos\psi\sin\psi}{r^2}-\frac{\psi'}{r}h\cos\psi+\frac{p}{2\kappa}rh\cos\psi\\ &+\frac{\gamma}{\kappa r}h^2\sin\psi+\frac{\eta}{\kappa r}h^2\cos\psi, \end{aligned} \tag{A3}$$

and two first-order equations

$$\gamma' = h\left[\frac{1}{2}\kappa\left(\frac{\psi'}{h}-c_0\right)^2-\frac{\kappa\sin^2\psi}{2r^2}+\sigma+pr\sin\psi\right], \tag{A4}$$

$$\eta' = 0, \tag{A5}$$

as well as the two geometric relations in Eq. (1).

In addition, the equation $\partial L/\partial h = 0$ does not give an equation of h, but leads to a conserved quantity[38,39]

$$\begin{aligned}\mathcal{H} \equiv \frac{\partial L}{\partial h} = &\frac{\kappa}{2}r\left[\left(\frac{\psi'}{h}\right)^2-\left(\frac{\sin\psi}{r}-c_0\right)^2\right]\\ &-\frac{p}{2}r^2\sin\psi-\sigma r+\gamma\cos\psi-\eta\sin\psi = 0. \end{aligned} \tag{A6}$$

There is a freedom to choose the scale function h. Here we choose $h' = 0$ such that h is a constant to be determined. It is essentially the total arclength of the membrane profile.

Appendix B: Derivation of the boundary conditions

By letting the boundary terms in Eq. (A2) equal to zero, we obtain the BCs. In particular, in the boundary term about δr, we let $\delta r|_{u=0}^{u=1} = 0$, which implies to fix the radius

$$r(0) = 0, \quad r(1) = R_{\mathrm{pore}}. \tag{B1}$$

In the boundary term about δz, we obtain

$$\frac{\partial L}{\partial z'}(u=0) = \eta(0) = 0, \quad z(u=1) = 0. \tag{B2}$$

As for the boundary term about $\delta\psi$, at the membrane tip, we have

$$\psi(0) = 0. \tag{B3}$$

At the pore edge, we have two choices. If we let $\delta\psi(1) = 0$, it is equivalent to the fixed-hinge BC

$$\psi(1) = 0. \tag{B4}$$

If we let $\partial L/\partial\psi' = 0$, it is equivalent to the free-hinge BC

$$\frac{\partial L}{\partial \psi'} = \kappa\left(\frac{\psi'}{h}+\frac{\sin\psi}{r}-c_0\right) = 0. \tag{B5}$$

The conserved quantity $\mathcal{H} = 0$ at the membrane tip $u = 0$ gives rise to a BC

$$\gamma(0) = 0. \tag{B6}$$

Appendix C: Numerical methods to calculate the D_{pore} vs. R_{pore} curve

So far we have obtained a total number of 5 equations, which include Eqs. (1), (A3), (A5). Since only Eq. (A3) is first order, they are equivalent to a total number of 6 first order ordinary differential equations. In addition, Eqs. (B1), (B2), (B3), (B4) or (B5), and (B6) constitute a total number of 7 BCs. Overall, the 6 equations plus 1 unknown parameter h, and the 7 BCs constitute a well-defined boundary value problem.

We solve the problem with the matlab solver bvp4c, which requires the equations and the BCs as its input. Furthermore, the solver requires an initial guess of the solutions. In order to obtain the D_{pore} vs. R_{pore} curve, We always start with a small R_{pore} and use the flat shape as our initial guess. In this case, the membrane is almost flat, and it is easy for the solver to find the solution. We then gradually increase the pore radius R_{pore} to $R_{\mathrm{pore}}+\Delta R$ and use the solution for R_{pore} as the initial guess to solve the equation for $R_{\mathrm{pore}}+\Delta R$. This iteration step allows us to extend the solution to the critical pore radius since beyond which no solutions are found anymore. We then use the solution at the critical pore radius as the starting point and iterate over the membrane depth D_{pore} to obtain the other branch of the solution. During this iteration, we add the boundary condition $z(0) = D_{\mathrm{pore}}$ and set the pore radius R_{pore} as an unknown parameter to be solved by the solver.

Acknowledgements

We acknowledge financial support from the National Natural Science Foundation of China (Grant No. 12004317), Fundamental Research Funds for Central Universities of China (Grant No. 20720200072), and 111 Project (Grant No. B16029).

References

[1] Mccann M C, Wells B and Roberts K 1990 *Journal of Cell Science* **96** 323
[2] Gong P, Taniguchi T and Ohshima M 2014 *Journal of Materials Science* **49** 2605
[3] Büquot; uttner F M, Faulhaber K, Forchhammer K, Maldener I and Stehle T 2016 *The FEBS Journal* **283** 1336
[4] Bacic A, Harris P J and Stone B A 1988 *The Biochemistry of Plants* **14** 297
[5] Keegstra K 2010 *Plant physiology* **154** 483
[6] Gow N A, Latge J P and Munro C A 2017 *Microbiology spectrum* **5** 10
[7] Free S J 2013 *Advances in genetics* **81** 33
[8] Silhavy T J, Kahne D and Walker S 2010 *Cold Spring Harbor perspectives in biology* **2** a000414
[9] Vollmer W, Blanot D and De Pedro M A 2008 *FEMS Microbiology Reviews* **32** 149
[10] Carpita N, Sabularse D, Montezinos D and Delmer D P 1979 *Science* **205** 1144
[11] Kirby A R, Gunning A P, Waldron K W, Morris V J and Ng A 1996 *Biophysical Journal* **70** 1138
[12] Nobel J and Barnett J A 1991 *Yeast* **7** 313
[13] Scherrer R, Louden L and Gerhardt P 1974 *Journal of Bacteriology* **118** 534
[14] Atilgan E, Magidson V, Khodjakov A and Chang F 2015 *Current biology: CB* **25** 2150
[15] Gualtieri T, Ragni E, Mizzi L, Fascio U and Popolo L 2004 *Yeast* **21** 1107
[16] Hohmann S 2002 *Microbiology and molecular biology reviews* **66** 300
[17] Hohmann S, Krantz M and Nordlander B 2007 *Methods in enzymology* **428** 29
[18] Rodríguez-Peña J M, García R, Nombela C and Arroyo J 2010 *Yeast* **27** 495
[19] Rojas E R and Huang K C 2018 *Current Opinion in Microbiology* **42** 62
[20] Ma R and Berro J 2021 *Biophysical Journal* **120** 52a
[21] Minc N, Boudaoud A and Chang F 2009 *Current Biology* **19** 1096
[22] Basu R, Munteanu E L and Chang F 2014 *Molecular biology of the cell* **25** 679
[23] Skruzny M, Brach T, Ciuffa R, Rybina S, Wachsmuth M and Kaksonen M 2012 *Proc. Natl. Acad. Sci. USA* **109** E2533
[24] Munglani G, Wittel F K, Vetter R, Bianchi F and Herrmann H J 2019 *Phys. Rev. Lett.* **123** 058002
[25] Knoche S and Kierfeld J 2014 *Soft Matter* **10** 8358
[26] Gordon V D, Chen X, Hutchinson J W, Bausch A R, Marquez M and Weitz D A 2004 *Journal of the American Chemical Society* **126** 14117
[27] Zong W, Li Q, Zhang X and Han X 2018 *Colloids and Surfaces B: Biointerfaces* **172** 459
[28] Nolte M, Dönch I and Fery A 2006 *ChemPhysChem* **7** 1985
[29] Yi-Ran L and Qing L 2019 *Acta Phys. Sin.* **68** 028701 (in Chinese)
[30] Jie S, Kai-Yu W, Bei-Bei M, Tao Z and Zhong-Ying J 2018 *Acta Phys. Sin.* **67** 2919 (in Chinese)
[31] Yang T, He D H, Zhang Q L and Ma H R 2005 *Acta Phys. Sin.* **54** 5937 (in Chinese)
[32] Wei T, Zhang L and Zhang Y 2020 *Chin. Phys. B* **29** 048702
[33] Liang Y F and Zahg S G 2017 *Acta Phys. Sin.* **66** 158701 (in Chinese)
[34] Zhang P W and Shi A C 2015 *Chin. Phys. B* **24** 128707
[35] Li S L and Zhang S G 2010 *Acta Phys. Sin.* **59** 5202 (in Chinese)
[36] Seifert U 1997 *Advances in Physics* **46** 13
[37] Zhang Y H, McDargh Z and Tu Z C 2018 *Chin. Phys. B* **27** 038704
[38] Seifert U, Berndl K and Lipowsky R 1991 *Phys. Rev. A* **44** 1182
[39] Jülicher F and Seifert U 1994 *Phys. Rev. E* **49** 4728
[40] Nezhad A S, Naghavi M, Packirisamy M, Bhat R and Geitmann A 2013 *Lab on a Chip* **13** 2599
[41] Pereira D, Alline T and Asnacios A 2022 *bioRxiv* 2022-12
[42] Stenson J D, Hartley P, Wang C and Thomas C R 2011 *Biotechnology progress* **27** 505
[43] Smith A, Moxham K and Middelberg A 2000 *Chemical Engineering Science* **55** 2043
[44] Chen X J and Liang Q 2017 *Chin. Phys. B* **26** 048701
[45] Helfrich W 1973 *Zeitschrift für Naturforschung C* **28** 693
[46] Agudo-Canalejo J and Nasouri B 2020 *Chin. Phys. B* **29** 064704
[47] Duan H, Li J F and Zhang H D 2018 *Acta Phys. Sin.* **67** 038701 (in Chinese)
[48] Di D D and Zhang S G 2018 *Acta Phys. Sin.* **67** 188701 (in Chinese)
[49] Meng F, Chen J Z, Doi M and Ouyang Z 2014 *AIChE Journal* **60** 1393
[50] Giudici A and Biggins J S 2020 *Europhys. Lett.* **132** 36001
[51] Giudici A and Biggins J S 2020 *Phys. Rev. E* **102** 033007
[52] Müller I, Strehlow P and Marder M 2005 *Physics Today* **58** 55
[53] Mallock A 1891 *Proc. Roy. Soc. Lond.* **49** 458
[54] Wang H, Zou B, Su J, Wang D and Xu X 2022 *Soft Matter* **18** 6015
[55] Shevchuk A I, Novak P, Taylor M, *et al.* 2012 *Journal of Cell Biology* **197** 499
[56] Tojkander S, Gateva G and Lappalainen P 2012 *Journal of cell science* **125** 1855
[57] Sekino Y, Kojima N and Shirao T 2007 *Neurochemistry international* **51** 92
[58] Faizi H A, Frey S L, Steinkühler J, Dimova R and Vlahovska P M 2019 *Soft Matter* **15** 6006
[59] Faizi H A, Tsui A, Dimova R and Vlahovska P M 2022 *Langmuir* **38** 10548
[60] Dimova R 2014 *Advances in colloid and interface science* **208** 225
[61] Barlow N E, Kusumaatmaja H, Salehi-Reyhani A, Brooks N, Barter L M, Flemming A J and Ces O 2018 *Journal of the Royal Society Interface* **15** 20180610
[62] Kozlov M M and Chernomordik L V 2015 *Current opinion in structural biology* **33** 61
[63] Gauthier N C, Masters T A and Sheetz M P 2012 *Trends in cell biology* **22** 527
[64] Lieber A D, Yehudai-Resheff S, Barnhart E L, Theriot J A and Keren K 2013 *Current biology* **23** 1409
[65] Kluge C, Pöhnl M and Böckmann R A 2022 *Biophysical Journal* **121** 671
[66] Różycki B and Lipowsky R 2015 *The Journal of Chemical Physics* **142** 02
[67] McMahon H T and Boucrot E 2015 *Journal of Cell Science* **128** 1065